Frustrated magnetism in the double perovskite La_2LiOsO_6: A comparison with La_2LiRuO_6

C. M. Thompson,[1] C. A. Marjerrison,[2] A. Z. Sharma,[3] C. R. Wiebe,[3] D. D. Maharaj,[2] G. Sala,[2] R. Flacau,[4] A. M. Hallas,[2] Y. Cai,[2] B. D. Gaulin,[2,5,6] G. M. Luke,[2,5,6] and J. E. Greedan[1,5]

[1]*Department of Chemistry and Chemical Biology, McMaster University, Hamilton, Canada L8S 4M1*
[2]*Department of Physics and Astronomy, McMaster University, Hamilton, Canada, L8S 4M1*
[3]*Department of Chemistry, University of Winnipeg, Winnipeg, Canada, R3B 2E9*
[4]*Canadian Neutron Beam Centre, Canadian Nuclear Laboratory, Chalk River, Canada, K0J 1J0*
[5]*Brockhouse Institute for Materials Research, McMaster University, Hamilton, Canada, L8S 4M1*
[6]*Canadian Institute for Advanced Research, Toronto, Canada, M5G 1Z8*

(Received 27 July 2015; revised manuscript received 8 December 2015; published 20 January 2016)

The frustrated double perovskite La_2LiOsO_6, based on Os^{5+} ($5d^3$, t_2^3) is studied using magnetization, elastic neutron scattering, heat capacity, and muon spin relaxation (μSR) techniques and compared with isostructural ($P2_1/n$) La_2LiRuO_6, Ru^{5+}($4d^3$, t_2^3). While previous studies of La_2LiOsO_6 showed a broad susceptibility maximum (χ_{max}) near 40 K, heat capacity data indicate a sharp peak at 30 K, similar to La_2LiRuO_6 with $\chi_{max} \sim 30$ K and a heat capacity peak at 24 K. Significant differences between the two materials are seen in powder neutron diffraction where the magnetic structure is described by $\boldsymbol{k} = (1/2\ 1/2\ 0)$ for La_2LiOsO_6, while La_2LiRuO_6 has been reported with $\boldsymbol{k} = (000)$, structure for face centered lattices. For the $\boldsymbol{k} = (1/2\ 1/2\ 0)$ structure, one has antiferromagnetic layers stacked antiferromagnetically, while for $\boldsymbol{k} = (0\,0\,0)$ structure, ferromagnetic layers are stacked antiferromagnetically. In spite of these differences, both can be considered as type I fcc antiferromagnetic structures. For La_2LiOsO_6, the magnetic structure is best described in terms of linear combinations of basis vectors belonging to irreducible representations Γ_2 and Γ_4. The combinations $\Gamma_2 - \Gamma_4$ and $\Gamma_2 + \Gamma_4$ could not be distinguished from refinement of the data. In all cases, the Os^{5+} moments lie in the yz plane with the largest component along y. The total moment is 1.81(4) μ_B. For La_2LiRuO_6, the Ru^{5+} moments are reported to lie in the xz plane. In addition, while neutron diffraction, μSR and NMR data indicate a unique $T_N = 24$ K for La_2LiRuO_6, the situation for La_2LiOsO_6 is more complex, with heat capacity, neutron diffraction, and μSR indicating two ordering events at 30 and 37 K, similar to the cases of cubic Ba_2YRuO_6 and monoclinic Sr_2YRuO_6.

DOI: 10.1103/PhysRevB.93.014431

I. INTRODUCTION

Interest in the class of materials known as *B*-site ordered double perovskite oxides has grown in recent years due in part to observations of unusual and unexpected magnetic behavior, such as the gapped spin singlet ground state of Ba_2YMoO_6, among others [1–3]. These compounds have the general composition $A_2BB'O_6$, where A is a large cation such as Ba^{2+}, Sr^{2+}, or La^{3+} and the B and B' cations are smaller ions that satisfy the stability constraints of the perovskite structure, according to the well-known tolerance factor, $t = [r\langle A\rangle + r(O)]/\sqrt{2}[(r\langle B\rangle + r(O)]$, where $r\langle A\rangle$ and $r\langle B\rangle$ are the average radii of the A-and B-site cations and $r(O)$ is the oxide ion radius [4]. If the difference in radius and formal charge between the B and B' ions is sufficiently large, these ions will occupy distinct crystallographic sites, the lattice topology of each being face centered [5]. If only the B' ion is magnetic, the potential for geometric magnetic frustration is present as the face centered lattice is one of edge-sharing tetrahedral [6]. The B' site ion is often from the 4*d* or 5*d* series and given the octahedral site geometry, the electronic configurations $nd^1(t_{2g}^1)$, $nd^2(t_{2g}^2)$ and $nd^3(t_{2g}^3)$ are common. In this study the $nd^3(t_{2g}^3)$ based double perovskites (DP) will be featured, in particular the isostructural, monoclinic ($P2_1/n$) compounds, La_2LiRuO_6 and La_2LiOsO_6, containing the magnetic ions $Ru^{5+}(4d^3)$ and $Os^{5+}(5d^3)$. This investigation mirrors studies of the closely related, isostructural, cubic (*Fm-3m*) phases Ba_2YRuO_6 and Ba_2YOsO_6 [7–9].

Table I below provides some context for the results to be presented. Here are collected relevant data for fourteen t_{2g}^3 DP materials for which t_{2g}^3 is the only magnetic ion and which have been reasonably well characterized, including neutron diffraction results. There are three B' ions involved, Ru^{5+}, Os^{5+}, and Ir^{6+}—the latter of which is not stable in a perovskite environment under ambient conditions and requires high pressure synthesis [15,16]. Some noteworthy results from Table I are that the majority of t_{2g}^3 DP materials show some type of long-range antiferromagnetic order(AFLRO), even those with rather large frustration indices f. Generally, the observed AFLRO is described by one of two wave vectors, $\boldsymbol{k} = (000)$ or $\boldsymbol{k} = (1/2\ 1/2\ 0)$. These are different magnetic structures that can be described in terms of the stacking of spin correlated planes normal to an unique axis. In the former, F planes are stacked with AF correlations to adjacent planes, while in the latter AF planes are stacked with AF correlations to the adjacent planes. Inspection of these structures yields the perhaps surprising observation that both can be classified as type I fcc, as the nearest-neighbor (nn) and next-nearest-neighbor (nnn) spin correlations are identical, namely, for n.n., there are 4 F and 8 AF, and for nnn, there are 6F. For cubic *Fm-3m* symmetry, only $\boldsymbol{k} = (0\,0\,0)$ is reported, while for monoclinic $P2_1/n$ symmetry, both wave vectors are found. Given the similarities in spin correlations, the two structures are likely very close in energy. There are only two exceptions to type I order, namely, La_2NaRuO_6, which orders with an incommensurate $\boldsymbol{k} = (0\,0\,0.091)$, and Ba_2LaRuO_6 with

TABLE I. Summary of relevant magnetic properties for fourteen t_{2g}^3 DP oxides.

DP	S.G.	θ_c(K)	T_N(K)	f*	Wave vector, $\boldsymbol{k}$	$\mu(B')\mu_B$**	Ref.
Sr_2YRuO_6	$P2_1/n$	–380	26	15	(0 0 0)	1.96(2)	[10]
Sr_2LuRuO_6	$P2_1/n$	–350	26	13	(0 0 0)	2.10(8)	[7]
La_2LiRuO_6	$P2_1/n$	–204	24	9	(0 0 0)	2.2(2)	[11]
La_2NaRuO_6	$P2_1/n$	–57	15	4	(0 0 0.091)	1.87(7)	[12]
Ba_2YRuO_6	*Fm-3m*	–571	36	16	(0 0 0)	2.2(1)	[7]
Ba_2LuRuO_6	*Fm-3m*	–630	35	18	(0 0 0)	2.06(8)	[7]
Ba_2LaRuO_6	*I-1*	–304	29	10	Type IIIa	1.96(10)	[13,14]
Ba_2YOsO_6	*Fm-3m*	–771	36	11	(0 0 0)	1.65(5)	[9]
Sr_2ScOsO_6	$P2_1/n$	–677	92	7	(0 0 0)	1.6(1)	[15]
Sr_2YOsO_6	$P2_1/n$	–313	53	6	(0 0 0)	1.91(3)	[16]
Sr_2InOsO_6	$P2_1/n$	–98	26	4	(0 0 0)	1.77(7)	[16]
La_2NaOsO_6	$P2_1/n$	–77	–	–	no order	–	[12]
Sr_2CaIrO_6	$P2_1/n$	–363	58	6	(1/2 1/2 0)	1.33(2)	[17]
Sr_2MgIrO_6	$P2_1/n$	–418	74?	6?	no order	–	[18]
Sr_2ZnIrO_6	$P2_1/n$	–430	46?	9?	no order	–	[18]

*$f = |\theta_c|/T_N$.
**Ordered moment on B' from neutron diffraction.
***$\boldsymbol{k}$ = (0 0 0.091),? indicates that T_N is assigned to an anomaly in the magnetic susceptibility but not confirmed by other probes.

type IIIa. The latter has triclinic crystallographic symmetry and is perhaps an outlier amongst the DP materials. Interestingly, three t_{2g}^3 DP materials do not order, La_2NaOsO_6, Sr_2MgIrO_6, and Sr_2ZnIrO_6.

It is worth noting that detailed studies have been reported for related DP materials with a t_{2g}^3 ion on the B' site but also with a magnetic ion on the *A* site. These were not included in Table I, as it is not clear what role is played by the A-site moment in the determination of the magnetic ground state. For example, in the Ru^{5+} series, Ln_2LiRuO_6, Ln = Pr, Nd, Gd, and Tb, all are reported to show a $\boldsymbol{k}$ = (1/2 1/2 0) state, with the exception of Ln = Gd, which does not appear to order to 2 K [19]. On the other hand, La_2LiRuO_6 has $\boldsymbol{k}$ = (000). Nd_2LiOsO_6 also belongs to the $\boldsymbol{k}$ = (1/2 1/2 0) group [20]. Finally, the ordered moments display a systematic dependence on the B' ion with average moments for Ru^{5+}, Os^{5+}, and Ir^{6+} of 2.1 μ_B, 1.7 μ_B, and 1.3 μ_B, respectively, which are lower than the nominal spin only value of 3 μ_B by about 30%, 43%, and 57%.

Returning to the two materials that are the subject of this work, while La_2LiRuO_6 is fairly well characterized by susceptibility, heat capacity and NMR, only the magnetic structure has been deduced from neutron diffraction and no detailed tracking of the order parameter nor any study of spin dynamics by muon spin relaxation (μSR) have been reported [11]. For the Os analog, only the crystal structure and bulk susceptibility data have been published [19]. Comparison of the cubic *Fm-3m* phases Ba_2YRuO_6 and Ba_2YOsO_6 showed some interesting systematics [8,9]. For example, T_N increased nearly twofold (36 to 69 K) upon replacement of the 4*d* Ru by 5*d* Os, which might be attributed to the larger radial extent of the 5*d* orbitals leading to enhanced magnetic exchange. The INS gap was also significantly larger for the Os analog, by a factor of 3.4. It was noted that this ratio is nearly the same as that for the free ion spin-orbit coupling (SOC) constants for Os^{5+} and Ru^{5+}, suggesting a role for this effect. The reduction in ordered moments by replacing Ru with Os has already been noted, which is another possible role for SOC. In fact, there exists a roughly linear correlation between the ordered moment measured by neutron diffraction and the free ion, one electron SOC constant, as seen in Fig. 1. However, correlation is not necessarily causation and a significant moment reduction can also be realized through the increased covalency or hybridization of the B'–O interaction involved in replacement of a 3*d* ion with one from the 4*d* or 5*d* series [15].

Studies to characterize La_2LiOsO_6 more fully using heat capacity, neutron diffraction, and μSR have been undertaken and are reported here along with μSR and further neutron elastic scattering investigations of La_2LiRuO_6 to permit a

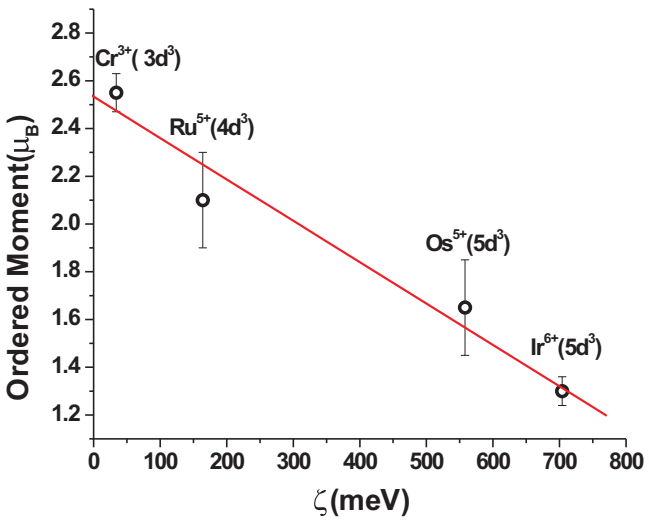

FIG. 1. Correlation between the ordered moments measured by neutron diffraction and the free ion, one electron SOC constant for nd^3 ions in a perovskite environment. The error bars represent the spread of values indicated in Table I. The SOC constants for Ru^{5+}, Os^{5+}, and Ir^{6+} are extrapolated from C.-G. Ma and M.G. Brik, J. Lumin. **145**, 402 (2014) and for Cr^{3+} from M. Blume and R.A. Watson, Proc. Roy. Soc. A270, 127 (1962).

TABLE II. Relevant structural data for $La_2LiB'O_6$.

	B' = Ru[11]	B' = Os[21]
a (Å)	5.5555(2)	5.5603(2)
b (Å)	5.5977(2)	5.6564(2)
c (Å)	7.8454(3)	7.8662(3)
B (deg)	90.020(5)	90.147(1)
V (Å^3)	243.98	247.40
B'–O1 (Å)	1.952(3)	1.957(4)
B'–O2 (Å)	1.959(3)	1.953(4)
B'–O3 (Å)	1.948(3)	1.964(4)
$\langle B'$–O$\rangle$ (Å)	1.953	1.958
$\langle B'$–O–Li$\rangle$ (deg)	155.1	153.5

detailed comparison of these two closely related DP materials. Results of inelastic neutron scattering studies of both materials will be presented in a separate publication.

II. EXPERIMENTAL

A. Sample preparation and characterization

La_2LiOsO_6 was prepared using a conventional solid state reaction. A mixture of La_2O_3, 10% excess of Li_2CO_3, and 10% excess of Os were ground together and heated in air for 2 hours at 900 °C with one intermittent regrinding. For La_2LiRuO_6, a mixture of La_2O_3, 10% excess of Li_2CO_3, and RuO_2 were ground together and heated in air for 1 day at 900 ^{o}C with one intermittent regrinding. Excess of Li_2CO_3 and Os were used to compensate for evaporation. A platinum crucible was used to avoid reaction with alumina. X-ray powder diffraction data showed single phase samples with unit cell constants in excellent agreement with the literature values given in Table II for each sample.

B. Magnetometry

Magnetic susceptibility was measured for La_2LiOsO_6 within the temperature range 2 to 300 K using a Quantum Design MPMS SQUID magnetometer at McMaster University. Zero-field cooling (ZFC) and field cooling (FC) data were obtained with an applied field of 0.05 T.

C. Heat capacity

Heat capacity measurements were performed using pellets of size 2–3 mg placed on a sapphire platform sample stage of a Dynacool Physical Property Measurement System (Quantum Design) equipped with a helium-3 heat capacity insert puck. The pellets were adhered to the platform using Apiezon N-grease during the measurements. The measurements were performed in 0 and 9-T fields for a temperature range of 0.350 and 300 K. The heat capacity of the puck and grease were subtracted from the total heat capacity.

D. Neutron elastic scattering

Neutron diffraction data without energy analysis were collected at the C2 instrument at the NRU reactor operated by the Canadian Nuclear Laboratory, Chalk River, Ontario, Canada.

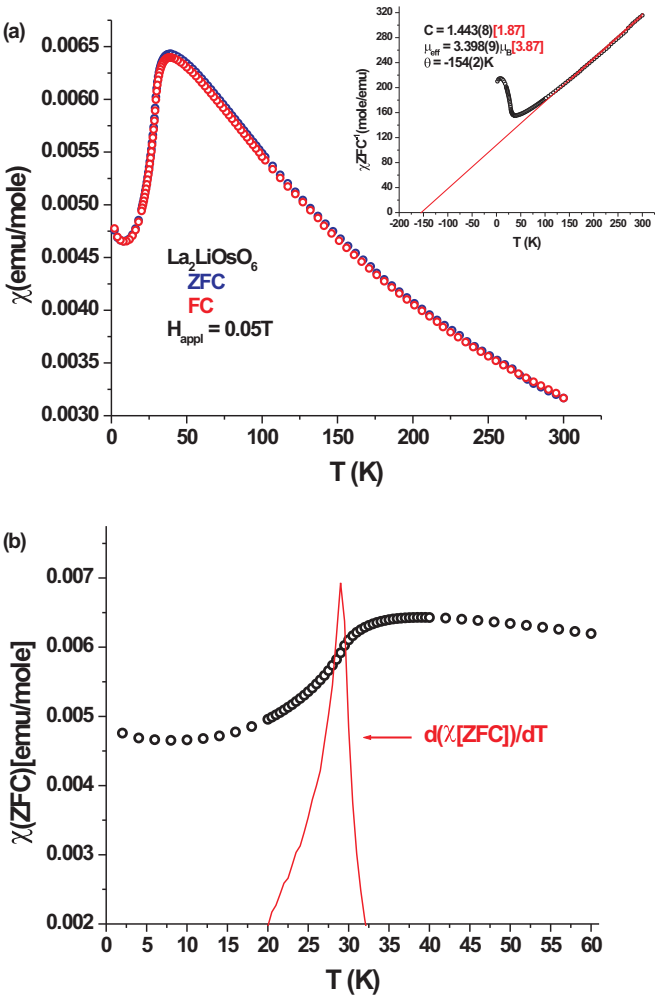

FIG. 2. (a) Magnetic susceptibility data for the La_2LiOsO_6 sample used in this study. The inset shows a Curie-Weiss analysis of the data, yielding $\mu_{\rm eff} = 3.398(9)\,\mu_{\rm B}$ and $\theta = -154(2)$ K, in good agreement with published data. The numbers in brackets are the spin only values for the Curie constant and the effective moment. Note that the ZFC and FC data are essentially indistinguishable. (b) The low-temperature susceptibility for La_2LiOsO_6 compared with $d\chi/dT$ vs T indicating that $T_{\rm N}$ is 30 K.

The data were collected at several temperatures from 3.5 to 280 K with neutron wavelengths of 2.3719 and/or 1.3305 Å depending on measurement temperature. The crystal and magnetic structures were refined using the FULLPROF suite of programs [22].

Neutron scattering measurements were also performed at the Spallation Neutron Source (SNS, Oak Ridge National Laboratory), on the SEQUOIA Fine Resolution Fermi Chopper Spectrometer [23]. For collection of elastic scattering data, an incident energy of 11 meV was used with an energy integration range from –0.15 to 0.15 meV. The samples were enclosed in annular aluminum cells with a He exchange gas atmosphere, loaded into an Orange 4He-flow cryostat, and investigated over a temperature range of 7 to 100 K. An identical empty can was measured under the same experimental conditions and used for background subtraction. Data reduction was accomplished using the software suite DAVE [24].

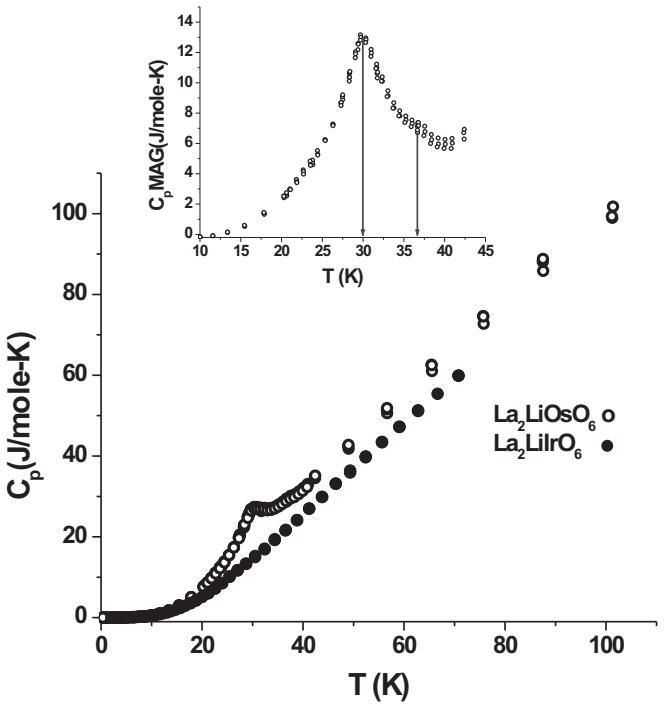

FIG. 3. Heat capacity for La_2LiOsO_6 compared with a lattice match phase, La_2LiIrO_6. The inset shows the magnetic contribution with a sharp maximum at 30 K and a weaker anomaly at ∼37 K.

E. μSR

Muon spin relaxation measurements were performed at the M20 surface muon channel at the TRIUMF Centre for Molecular and Materials Science Facility. The samples were mounted in a low-background insert in a helium gas flow cryostat, such that muons not landing in the sample were not recorded in the collected spectra.

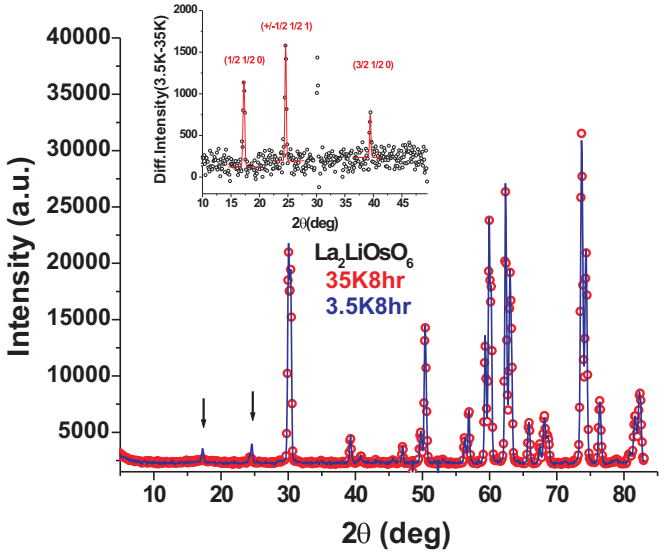

FIG. 4. A comparison of neutron diffraction data, $\lambda = 2.37$ Å, for La_2LiOsO_6 at 3.5 K (blue line) and 35 K (red circles). Two magnetic peaks are indicated by arrows. The inset shows a difference plot, 3.5–35 K, from which a third magnetic peak can be detected.

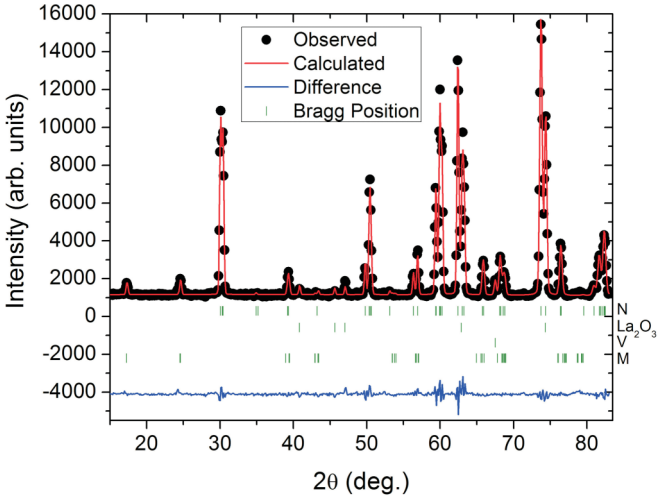

FIG. 5. Rietveld refinement of the neutron diffraction pattern of La_2LiOsO_6 at 3.5 K including the magnetic structure—a linear combination of the basis vectors of the Γ_2 and Γ_4 irreducible representations—lowest tick marks. See text for further information. Reflections from a small La_2O_3 impurity and the vanadium sample can are also indicated.

III. RESULTS AND DISCUSSION

A. Crystal structure

Both La_2LiRuO_6 and La_2LiOsO_6 crystallize in a monoclinic perovskite structure with symmetry $P2_1/n$ and the unit cell constants and some relevant interatomic distances and angles are listed in Table II. Note that the unit cell volumes differ by only 1.4% and that the B'–O distances are equal to within 2σ, i.e., there is very little distortion of the coordination octahedron of B' in either material. The B'–O–Li angles, critical for the super-super exchange interactions, differ by less than 2°. The slightly larger cell volume for the Os phase is consistent with the slightly larger radius of Os^{5+}(0.575 Å) relative to Ru^{5+}(0.565 Å) [25]. From a structural perspective these are two very similar materials.

B. Magnetic susceptibility

The published magnetic susceptibility data for La_2LiRuO_6 and La_2LiOsO_6 show similar features, including relatively large negative Curie-Weiss temperatures of –207 and –168 K and broad susceptibility maxima at ∼30 and ∼40 K, respectively [11,21].

Data were collected for the La_2LiOsO_6 sample used in this study and the results are shown in Figs. 2(a) and 2(b). Note first the broad maximum near 40 K and that the ZFC and FC data can be superimposed. Thus no canted moment exists in spite of the fact that the D-M interaction is permitted for DP materials with $P2_1/n$ symmetry. The derived Curie-Weiss parameters [inset Fig. 1(a)], $\mu_{\text{eff}} = 3.398(9)\,\mu_B$ and $\theta = -154(2)$ K, are in reasonable agreement with published data [21]. Note that μ_{eff} is somewhat reduced, ∼12%, from the spin only value, 3.87 μ_B. In Fig. 2(b), an attempt is made to locate T_N by

TABLE III. Refined magnetic structure models and magnetic moment for La_2LiOsO_6.

	$\Gamma_2+\Gamma_4$	$\Gamma_2+\Gamma_4$	$\Gamma_2+\Gamma_4$	$\Gamma_2-\Gamma_4$	$\Gamma_2-\Gamma_4$	$\Gamma_2-\Gamma_4$
B_1'	$[q_1, q_2, q_3]$	$[q_1, q_2, q_3]$	$[q_1, q_2, q_3]$	$[q_1, q_2, q_3]$	$[q_1, q_2, q_3]$	$[q_1, q_2, q_3]$
B_2'	$[-r_1, r_2, -r_3]$	$[-r_1, r_2, -r_3]$	$[-r_1, r_2, -r_3]$	$[r_1, -r_2, r_3]$	$[r_1, -r_2, r_3]$	$[r_1, -r_2, r_3]$
Os						
μ_x	−0.2(2)	0 (fixed)	0 (fixed)	−0.2(2)	0 (fixed)	0 (fixed)
μ_y	1.6(2)	1.72(8)	1.79(4)	1.6(2)	1.72(8)	1.79(4)
μ_z	0.8(3)	0.4(2)	0 (fixed)	0.8(3)	0.5(2)	0 (fixed)
μ_{Total}, μ_B	1.84(3)	1.79(6)	1.79(4)	1.84(3)	1.79(6)	1.79(4)
R_{mag}, %	23.0	24.8	25.5	23.0	24.3	25.0

plotting $d\chi/dT$ and a sharp maximum is seen at 30 K. It was shown conclusively from heat capacity and nmr studies that for the Ru phase, $T_N = 24$ K, while T_N had not been reported previously for the Os analog [8].

C. Heat capacity

Heat capacity data for La_2LiOsO_6 are shown in Fig. 3 along with those for a lattice match material, La_2LiIrO_6. $Ir^{5+}(5d^4)$ is nonmagnetic in this phase [26]. While the lattice match is not ideal, it is possible to isolate an approximate magnetic contribution shown in the inset. Note the sharp maximum just below 30 K, in excellent agreement with the analysis of Fig. 2(b), but also a much weaker anomaly near 37 K. The total entropy lost over the investigated temperature range is 8.47 J/mole K^2, which is 73% of that expected for $S = 3/2$, 11.66 J/mole K^2. Thus the true T_N appears to be well below the susceptibility maximum of ∼40 K, very similar to the case for La_2LiRuO_6.

D. Neutron diffraction

As mentioned, elastic neutron scattering data were collected both at the C2 diffractometer and SEQUOIA for the Os phase and only at SEQUOIA for the Ru analog. Analysis of C2 data for La_2LiOsO_6 will be discussed first.

Data were taken from 3.5 to 35 K and a comparison of results for these terminal temperatures is shown in Fig. 4. Two magnetic reflections are readily detected, marked by arrows. From a difference plot, 3.5–35 K, three magnetic peaks were found, see the inset. These reflections were indexed using the k-search function of Fullprof, and $\boldsymbol{k} = (1/2\ 1/2\ 0)$ was found, unequivocally, instead of the expected $\boldsymbol{k} = (0\ 0\ 0)$, which describes the magnetic structures of the majority of nd^3 DP materials, including La_2LiRuO_6, as noted in Table I. In fact, the only other DP in this class with $\boldsymbol{k} = (1/2\ 1/2\ 0)$ is Sr_2CaIrO_6 although, as mentioned previously, it is found for some nd^3 DP materials with magnetic ions on the A site.

In order to determine possible magnetic structures suitable for the space group $P2_1/n$, the program SARAH was employed for representational analysis [27]. For $\boldsymbol{k} = (1/2\ 1/2\ 0)$, this resulted in two irreducible representations (IR), Γ_2 and Γ_4 (in Kovalev's notation). The IRs Γ_2 and Γ_4, describe the magnetic spins within different layers. For La_2LiRuO_6, it was determined that the magnetic structure consisted of moments ordering in both layers and the same assumption was made for the La_2LiOsO_6 case. Hence the refinement of the neutron diffraction data was undertaken by combining the basis vectors (BV) of Γ_2 with Γ_4 (Fig. 5) and this provided two possible symmetry allowed magnetic structures ($\Gamma_2+\Gamma_4$ and $\Gamma_2-\Gamma_4$; Table III). The refinements revealed that both models fit the data equally well and are indistinguishable with the existing data. In all cases the x component is zero and the major component is along y with a small component along z. The refined Os^{5+} total magnetic moment (the average of all of the models) is 1.81(4) μ_B (Table IV), which is significantly smaller than the expected ordered moment for an $S = 3/2$ ion, but similar to experimental values reported for other osmium double perovskites, Table I. The refined magnetic structure is shown in Fig. 6.

As mentioned, elastic neutron powder data are also available for both the Ru and Os DP compounds from the SEQUOIA experiments, albeit with lesser Q resolution. These results are nonetheless highly instructive regarding the differences in magnetic structure and also in the behavior of the order parameter as seen in Fig. 7. Note first Figs. 7(a) and 7(b), the obvious differences in relative intensities of the two strongest magnetic reflections, which are illustrative of the different magnetic structures described by $\boldsymbol{k} = (0\ 0\ 1)$ for the Ru DP and $\boldsymbol{k} = (1/2\ 1/2\ 0)$ for the Os analog. A more surprising difference is seen in the behavior of the order parameter. While for the Ru phase the data are quite consistent with $T_N = 24$ K, in the case of Os there is nonzero magnetic intensity persisting to temperatures higher than 30 K, indicating a secondary ordering just below 37 K, consistent

TABLE IV. Neutron diffraction refinement results of the crystal structure of La_2LiOsO_6 at 3.5 K.

Atom	x	y	Z	B_{iso}(Å^2)
La	0.489(9)	0.047(6)	0.248(5)	0.25
Li	0	0	0	0.37
Os	0.5	0.5	0	0.25
O1	0.218(9)	0.29(1)	0.04(1)	0.2
O2	0.58(1)	0.481(8)	0.245(8)	0.2
O3	0.305(9)	0.78(1)	0.046(9)	0.2
a (Å)	5.5443(4)			
b (Å)	5.6312(4)			
c (Å)	7.8440(7)			
β (°)	90.199(3)			

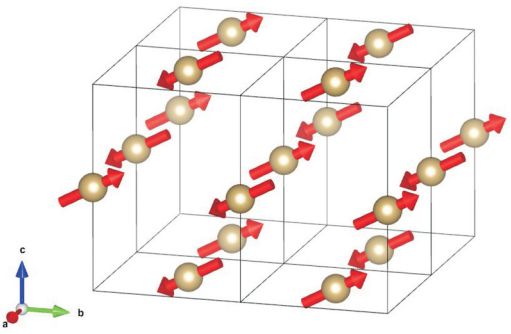

FIG. 6. The magnetic unit cell of La_2LiOsO_6. Osmium atoms are shown in gold. Lanthanum, lithium, and oxygen atoms are omitted for clarity and the red arrows represent the Os^{5+} magnetic moments. See text for further information.

with the heat capacity data. This behavior is reminiscent of the situation for Ba_2YRuO_6 and Sr_2YRuO_6 both of which showed two apparent orderings at 36 and 47 K and 24 and 30 K, respectively [28–31]. For Ba_2YRuO_6, it was shown that the region between 36 and 47 K was dominated by shorter-range spin correlations [29]. It is presently unclear whether shorter-range spin correlations are also present in La_2LiOsO_6 in the 30–37 K range. The existing neutron diffraction data are not of sufficient quality to provide a definitive answer.

E. μSR

μSR can provide information which is complementary to that of neutron diffraction in terms of the order parameter. The temperature dependence of the asymmetry parameter for both the Ru and Os DP materials is shown in Fig. 8. The solid line is a fit to four relaxation processes as indicated in

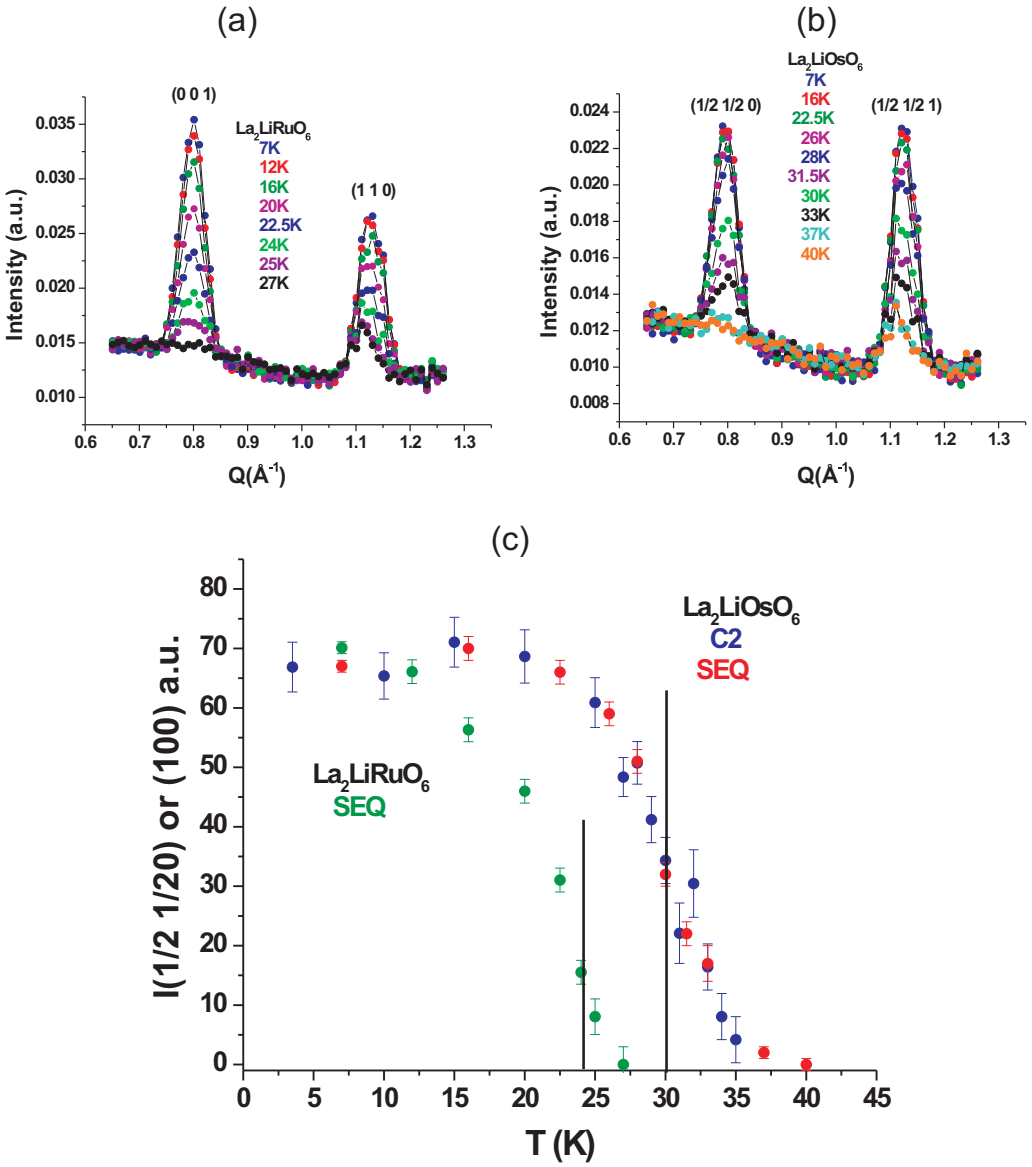

FIG. 7. (a) Magnetic reflections at several temperatures for La_2LiRuO_6. (b) Magnetic reflections at several temperatures for La_2LiOsO_6. (c) The order parameters for La_2LiRuO_6 and La_2LiOsO_6. For the latter, data are also included from the C2 experiments. The vertical black lines indicate the position of the sharp anomaly in the heat capacity data.

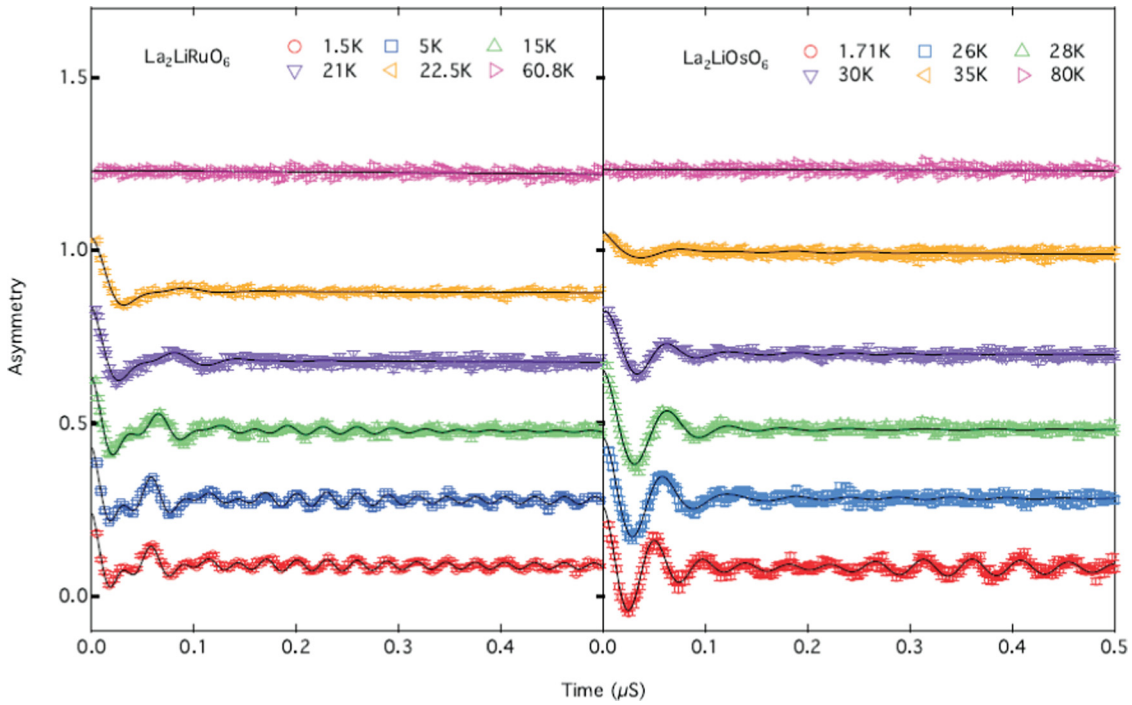

FIG. 8. The asymmetry parameter for La_2LiRuO_6 (left) and La_2LiOsO_6 (right) vs temperature. Note the presence of oscillations arising from unique, static internal fields, consistent with the onset of long-range magnetic order in both materials with decreasing temperature. The fits are to the function indicated in the text.

Eq. (1),

$$\begin{aligned}\text{Assym.} = {} & A_1 \cos[\omega_1(B_1)t + \varphi_1]e^{-\lambda(1)/t} \\ & + A_2 \cos[\omega_2(B_2)t + \varphi_2]e^{-\lambda(2)/t} \\ & + A_3 \cos[\omega_3(B_3)t + \varphi_2]e^{-\lambda(3)/t} + A_4 e^{-\lambda(4)/t},\end{aligned} \tag{1}$$

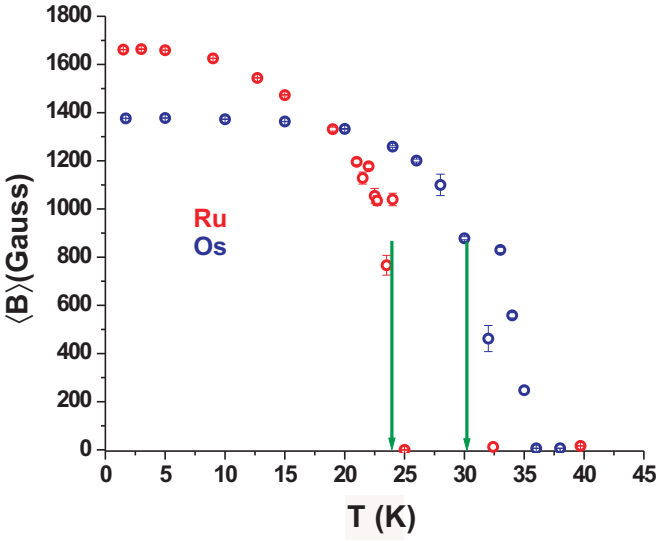

FIG. 9. Temperature dependence of $\langle B_i \rangle$ for La_2LiRuO_6 (red) and La_2LiOsO_6 (blue). $\langle B_i \rangle$ is defined as $\langle B_i \rangle = (A_1B_1 + A_2B_2 + A_3B_3)/A_{\text{total}}$. The vertical arrows indicate the temperatures at which sharp heat capacity anomalies occur.

where A_i are amplitudes, ω_i are muon precession frequencies, B_i are local fields at the muon sites, and λ_i are the relaxation rates. Note that there are three frequencies/internal fields indicating the existence of three muon sites which is in turn consistent with the presence of three O sites in the $P2_1/n$ DP structure.

In Fig. 9, the temperature dependence of $\langle B_i \rangle$, defined as $\langle B_i \rangle = (A_1B_1 + A_2B_2 + A_3B_3)/A_{\text{total}}$, is plotted for both the Ru and Os DP phases, which can be taken as an order parameter for each. Note that the data for La_2LiRuO_6 indicate $T_N = 24$ K, consistent with that from the neutron diffraction, Fig. 7(c), in addition to heat capacity and NMR data from previous studies [8]. In contrast for La_2LiOsO_6, $\langle B_i \rangle$ shows a significant dip near ~30 K, the position of the sharp heat capacity anomaly and vanishes near 37 K, consistent with the elastic neutron scattering results and the weak heat capacity anomaly. Also the ratio of the saturation value of $\langle B_i \rangle$ for the Ru and Os DP phases ~1682 G/1377 G = 1.2 is equal to the ratio of the ordered moments obtained from neutron diffraction, 2.2 μ_B/1.8 μ_B = 1.2. This is reasonable as the magnetic field seen by the muon should be linearly related to the magnetic moments. which give rise to this field.

IV. SUMMARY AND CONCLUSIONS

La_2LiRuO_6 and La_2LiOsO_6 are structurally very similar, both crystallize in $P2_1/n$ with unit cell volumes that differ by only 1.4%. Magnetic susceptibility data for both show broad maxima at ~30 K (Ru) and ~40 K (Os) but AF long-range order sets in below 24 K (Ru) and 30 K(Os) with an indication

of an additional ordering near 37 K for the Os phase, which is detected by heat capacity, neutron diffraction and μSR. While the nearly ubiquitous magnetic structure, $\boldsymbol{k} = (0\,0\,0)$, is found for the Ru phase, for the Os compound, a different magnetic ground state, described by $\boldsymbol{k} = (1/2\,1/2\,0)$, pertains. As noted previously, the $\boldsymbol{k} = (0\,0\,0)$ structure can be described as F layers stacked in an AF sequence, while for $\boldsymbol{k} = (1/2\,1/2\,0)$, AF layers are stacked in an AF sequence. The origin of this difference in magnetic structure is currently unclear. As already emphasized, the difference in energy between these two ground states is likely to be small. In La_2LiRuO_6, the stacking direction is the c axis with moment components in the ac plane and a total moment of $2.2(2)\mu_B$ while for La_2LiOsO_6 the stacking direction is the same but the moment components are in the bc plane with a total value of $1.81(4)\mu_B$. This moment reduction could reflect either the greater influence of SOC or covalency effects upon replacing a $4d$ ion with a $5d$ ion. There are also interesting comparisons with the cubic analogs, Ba_2YRuO_6 and Ba_2YOsO_6. Here, the ground state for both materials is $\boldsymbol{k} = (000)$. The enhancement in T_N upon replacement of the $4d$ ion Ru with the $5d$ ion Os, is much greater, $68/36 = 1.9$, while for the monoclinic materials, this factor is only 1.25. This may reflect the more efficient super-super-exchange pathways available in the cubic structure materials, as all of the angles involved in the Ru(Os) –O-Y-O–Ru(Os) pathway angles are 180° for J_{nnn} and for J_{nn} the O–Y–O angle is 90°. For the $P2_1/n$ phases, some of these are much more acute, with Ru(Os)–O-Li angles of ∼154° for both J_{nn} and J_{nnn}. On the other hand, the O–Li–O angle is ∼90° for J_{nn} and ∼180° for J_{nnn}.

ACKNOWLEDGMENTS

J.E.G., G.M.L., C.R.W., and B.D.G. thank the Natural Sciences and Engineering Research Council of Canada for support via the Discovery Grant Program. C.R.W. also acknowledges support from the Canadian Foundation for Innovation and the Canada Research Chair program,Tier II. P. Dube assisted with collection of magnetization data. We thank the TRIUMF CMMS staff for invaluable assistance with the μSR experiments. Research at Oak Ridge National Laboratory's Spallation Neutron Source was sponsored by the Scientific User Facilities Division, Office of Basic Energy Sciences, US Department of Energy.

[1] T. Aharen, J. E. Greedan, C. A. Bridges, A. A. Aczel, J. Rodriguez, G. MacDougall, G. M. Luke, T. Imai, V. K. Michaelis, S. Kroeker, C. R. Wiebe, H. Zhou, and L. M. D. Cranswick, Phys. Rev. B **81**, 224409 (2010).

[2] M. A. de Vries, A. C. Mclaughlin, and J.-W. G. Bos, Phys. Rev. Lett. **104**, 177202 (2010).

[3] J. P Carlo, J. P. Clancy, T. Aharen, Z. Yamani, J. P. C. Ruff, J. J. Wagman, G. J. Van Gastel, H. M. L. Noad, G. E. Granoth, J. E. Greedan, H. A. Dabkowska, and B. D. Gaulin, Phys. Rev. B **84**, 100404 (2011).

[4] V. M. Goldschmidt, Die Naturwissenschaften **14**, 477 (1926).

[5] M. T. Anderson, K. B. Greenwood, G. A. Taylor, and K. R. Poeppelmeier, Prog. Solid State Chem. **22**, 197 (1993).

[6] A. P. Ramirez, Ann. Rev. Mat. Sci. **24**, 453 (1994).

[7] P. D. Battle and C. W. Jones, J. Solid State Chem. **78**, 108 (1989).

[8] T. Aharen, J. E. Greedan, F. Ning, T. Imai, V. Michaelis, S. Kroeker, H. Zhou, C. R. Wiebe, and L. M. D. Cranswick, Phys. Rev. B **80**, 134423 (2009).

[9] E. Kermarrec, C. A. Marjerrison, C. M. Thompson, D. D. Maharaj, K. Levin, S. Kroeker, G. E. Granroth, R. Flacau, Z. Yamani, J. E. Greedan, and B. D. Gaulin, Phys. Rev. B **91**, 075133 (2015).

[10] P. D. Battle and W. J. Macklin, J. Solid State Chem. **52**, 138 (1984).

[11] P. D. Battle, C. P. Grey, M. Hervieu, C. Martin, C. A. Moore, and Y. Park, J. Solid State Chem. **175**, 20 (2003).

[12] A. A. Aczel, D. E. Burgaris, L. Li, J.-Q Yan, C. De la Cruz, H.-C. zur Loye, and S. E. Nagler, Phys. Rev. B **87**, 014435 (2013); A. A. Aczel, P. J. Baker, D. E. Bulgaris, J. Yeon, H.-C. zur Loye, T. Guidi, and D. T. Adroja, Phys. Rev. Lett. **112**, 117603 (2014).

[13] R. Greatrex, N. N. Greenwood, M. Lai, and I. Fernandez, J. Solid State Chem. **30**, 137 (1979).

[14] P. D. Battle, J. B. Goodenough, and R. Price, J. Solid State Chem. **46**, 234 (1983).

[15] A. E. Taylor, R. Morrow, D. J. Singh, S. Calder, M. D. Lumsden, P. M. Woodward, and A. D. Christianson, Phys. Rev. B **91**, 100406(R) (2015).

[16] A. K. Paul, A. Sarapulova, P. Adler, M. Reehuis, S. Kanungo, D. Mikhailova, W. Schelle, Z. Hui, C. Kuo, V. Siruguri, S. Rayaprol, Y. Soo, B. Yan, C. Felser, L. H. Tjeng, and M. Jansen, Z. Anorg. Allgem. Chem. **641**, 197 (2015).

[17] P. Kayser, M. J. Martinez-Lopez, J. A. Alonso, M. Retuerto, M. Croft, A. Ignatov, and M. T. Fernandez-Diaz, Eur. J. Inorg. Chem. 178 (2014).

[18] P. Kayser, M. J. Martinez-Lopez, J. A. Alonso, M. Retuerto, M. Croft, A. Ignatov, and M. T. Fernandez-Diaz, Inorg. Chem. **52**, 11013 (2013).

[19] S. J. Makowski, J. A. Rodgers, P. F. Henry, J. P. Attfield, and J.-W. G. Bos, Chem. Mater. **21**, 264 (2009).

[20] A. A. Aczel, D. E. Burgaris, J. Yeon, C. de la Cruz, H.-C. zur Loye, and S. E. Nagler, Phys. Rev. B **88**, 014413 (2013).

[21] W. R. Gemmill, M. D. Smith, and H.-C. zur Loye, J. Solid State Chem. **179**, 1750 (2006).

[22] J. Rodriguez-Carvajal, Physica B **192**, 55 (1993).

[23] G. E. Granroth, A. I. Kolesnikov, T. E. Sherline, J. P. Clancy, K. A. Ross, J. P. C. Ruff, B. D. Gaulin, and S. E. Nagler, J. Phys. Conf. Ser. **251**, 012058 (2010).

[24] R. T. Azuah, L. R. Kneller, Y. Qui, P. L. W. Tregenna-Piggott, C. M. Brown, J. R. D. Copley, and R. M. Dimeo, J. Res. Natl. Inst. Stan. Technol. **114**, 341 (2009).

[25] R. D. Shannon, Acta. Cryst. A **32**, 751 (1976).

[26] K. Hayashi, G. Demazeau, M. Pouchard, and P. Hagenmuller, Mat. Res. Bull. **15**, 461 (1980); J. Darriet, G. Demazeau, and M. Pouchard, *ibid.* **16**, 1013 (1981).
[27] A. S. Wills, Physica B **276–278**, 680 (2000).
[28] J. P. Carlo, J. P. Clancy, K. Fritsch, C. A. Marjerrison, G. E. Granroth, J. E. Greedan, H. A. Dabkowska, and B. D. Gaulin, Phys Rev. B **88**, 024418 (2013).
[29] G. J. Nilsen, C. M. Thompson, G. Ehlers, J. E. Greedan, C. A. Marjerrison, and J. E. Greedan, Phys. Rev. B **91**, 054415 (2015).
[30] R. P. Singh and C. W. Tomy, Phys. Rev. B **78**, 024432 (2008).
[31] E. Granado, J. W. Lynn, R. F. Jardim, and M. S. Torikachvili, Phys. Rev. Lett. **110**, 017202 (2013).